Designing Squaraines to Control Charge Injection and Recombination Processes in NiO-based Dye-Sensitized Solar Cells

(Article begins on next page)

19 February 2025

Designing Squaraines to Control Charge Injection and Recombination Processes in NiO-based Dye-Sensitized Solar Cells

Oliver Langmar,[a] Davide Saccone,[b] Anna Amat,[c] Simona Fantacci,[c] Guido Viscardi,[b] Claudia Barolo,* [b] Rubén D. Costa* [a] and Dirk M. Guldi* [a]

a]   O.Langmar, Dr. R.D.Costa, Prof. D.M.Guldi Department of Chemistry and Pharmacy Friedrich-Alexander-Universität Erlangen-Nürnberg Egerlandstr. 3, 91058 Erlangen, Germany E-mail: ruben.costa@fau.de, dirk.guldi@fau.de

b]   D.Saccone, Prof. G.Viscardi, Prof. C.Barolo INSTM Reference Centre University of Torino Via Pietro Giuria 7, 10125 Torino, Italy E-mail: claudia.barolo@unito.it

[c]   Dr. A.Amat, Dr. S.Fantacci Computational Laboratory for Hybrid/Organic Photovoltaics (CLHYO) CNR-ISTM Via Elce di Sotto 8, 06123 Perugia, Italy

Abstract: Herein, the synthesis of a novel family of squaraines (SQ) and their application in p-type dye-sensitized solar cells (DSSC) is presented. In particular, two sets of SQs were designed featuring either two or four anchoring carboxylic groups combined with either oxygen or dicyanovinyl central groups. The SQs have been characterized by using a joint theoretical, photophysical and electrochemical approach. Importantly, the presence of different central groups forces them into a frozen *cis* (dicyanovinyl group) or a *trans* (oxygen group) conformation. Based on the latter, the current work enables the direct comparison between *cis* and *trans* isomers, as well as the impact of a different number of anchors. Considering their electron accepting and light harvesting character they were tested in NiO-based DSSCs. Photocurrent-voltage, incident photon-to-current conversion efficiency, and electrochemical impedance spectroscopy measurements were performed. By virtue of their different symmetry, stereochemistry, and number of carboxylic groups, altered adsorption behavior onto NiO electrodes, as well as diverse charge injection and charge recombination dynamics were noted under operation conditions. SQs with four linkers in a frozen *cis* isomery show the best charge collection properties among the investigated SQs, providing a valuable guideline for the molecular design of future SQs for p-type DSSCs. As a complement, we assembled tandem-DSSCs featuring SQ / NiO photocathodes and N719 / TiO$_2$ photoanodes. The IPCE of the resulting tandem-DSSCs imply light harvesting throughout most of the visible part of the solar spectrum due to the complementary absorption of SQ and N719.

Introduction

Owing to the ever-increasing demand for energy, new ways are sought to optimize the power conversion of solar technology. To this end, the dye-sensitized solar cell (DSSC) concept is a leading example.[1] A promising approach to increase the conversion efficiency is the design of tandem DSSCs (t-DSSCs), which combine both n- and p-type DSSCs using, for example, TiO$_2$-based photoanodes and NiO-based photocathodes, respectively.[2–5] In a t-DSSC device configuration, both electrodes are decorated with photosensitizers featuring complementary light harvesting properties, covering a maximum range of the visible region of the solar spectrum.[2] Up to date, the efficiency of t-DSSCs seems to be limited by the performance of the photocathode. In contrast to n-type DSSCs, research on p-type based DSSCs is still in its infancy with maximum efficiencies of only 0.6% and 2.51 % for the I$^-$/I$_3^-$ and Fe^{2+}/Fe^{3+}-based redox couple, respectively.[6,7]

Current activities in the area of p-type DSSCs focus on developing novel photosensitizers to improve the general device performance.[8–13] Here, a number of key requirements need to be met: (i) a broad absorption spectrum with a high extinction coefficient should be guaranteed; (ii) the highest-occupied molecular orbital (HOMO) energy of the sensitizer must lie below the valence band (VB) energy of the p-type semiconductor; (iii) the lowest-unoccupied molecular orbital (LUMO) energy should be placed above the redox potential of the electrolyte to ensure efficient electron injection and regeneration, respectively; (iv) a high photo- and thermal-stability is required.[14] Considering that one of the most efficient dyes for photoanodes are based on Ruthenium(II) complexes,[15] which absorb in the high-energy region of the visible spectrum, a matching photosensitizer for photocathodes in a t-DSSC should harvest light in the low-energy region. In this context, squaraines (SQ) have been widely investigated as near infrared (NIR) light harvesters. As a matter of fact, SQs have turned into promising sensitizers for n-type DSSCs with remarkable efficiencies.[16] This is in stark contrast to the lack of examples for SQs applied in NiO-based DSSCs.[17,18] As a matter of fact, since SQs show high extinction coefficients, excellent photostabilities due to the rigidity of the squaraine core, and easy tunability of their molecular and electronic structures,[19] they seem to fulfill most of the aforementioned key requirements.

As shown in research on n-type DSSC, the symmetry and number of carboxylic groups of the SQ-photosensitizers exerts a drastic impact on the charge injection and/or recombination processes under operation conditions, resulting in a high impact on the device figures-of-merit. Here, the use of VG1 and VG10 resulted in energy conversion efficiencies of 4.6% and 6.1%, respectively.[20,21]

In the current work, we provide insights into the design of SQs as integrative components for p-type DSSCs, which is, to the best of our knowledge, absent in the literature. We opted for the synthesis of two novel families of SQs - see **Figure 1** – which differ in their structural conformation due to the nature of the central group – oxygen (**O**) *versus* dicyanovinyl (**CN**) – and the number of carboxylic anchoring groups - two (**2**) *versus* four (**4**). On one hand, unsymmetric (**O2** and **CN2**) and symmetric (**O4** and **CN4**) SQs are compared to investigate the impact of the number of anchoring groups. On the other hand, introducing the CN central moiety allows the control over the molecular stereoisomery, showing either a *cis/trans* equilibrium (**O2** and **O4**) or a frozen *cis* structure (**CN2** and **CN4**). All SQs were investigated by theoretical, photophysical, and electrochemical characterization, and they were employed as photosensitizers in NiO-based DSSCs. Based on current-voltage (J-V), incident photon-to-current conversion efficiency (IPCE), and electrochemical impedance spectroscopy (EIS) assays, we document that the symmetry and the preferred stereo-conformation of the SQs rule the adsorption behavior and, in turn, the charge injection and recombination processes under device operation conditions. Finally, we assembled tandem-DSSCs featuring SQ / NiO photocathodes and N719 / TiO$_2$ photoanodes and, in turn, panchromatic absorption.

Results and Discussion

Synthesis

The structures of **O2**, **O4**, **CN2**, and **CN4** are based on the combination of an electron accepting squaric core and either one or two electron donating biphenylamines. The incentive for their synthesis is to shed some light onto the number of carboxylic anchoring groups and the structural isomerism on the performance of p-type DSSCs.

To maximize the synthetic yields we have modified the previously published procedure by Chang *et al.* on the synthesis of SQs for NiO-based p-type DSSCs.[17] In particular, we replaced the

Figure 1. Molecular structures of novel SQ-sensitizers **O2**, **O4**, **CN2**, and **CN4**.

Suzuki coupling reaction by a Buchwald-Hartwig coupling reaction to link an indolenine moiety to biphenylamine. This helps to reduce the number of synthetic steps to two and places the squaric core between the biphenylamine and the indolenine moieties. Noteworthy, the synthesis of symmetrical SQs is more efficient in terms of time, use of reagents, and costs than the asymmetrical ones, since the formation of hemisquarate intermediates and their subsequent hydrolysis is circumvented. However, it is still under debate in the design of SQs for n-type DSSCs, if asymmetrical dyes might enhance the device performance compared to the symmetric ones.[20,21] In this context, the use of a microwave heating in a series of synthesis steps, such as indolenine formation and relative alkylation,[22] palladium-catalyzed heterocoupling reactions, and squarate substitution has enabled to avoid the hydrolysis step between the hemisquarate intermediate and the squaraine formation in the preparation of asymmetric squarines, reducing the reaction time, and enhancing the overall yield.[23]

To sum up the synthesis protocol, 5-bromoindolenine has been synthesized by a Fisher indole reaction starting from 4-bromophenylhydrazine. In the next step, 5-bromoindolenine has been alkylated on the nitrogen with iodoethane and put in reaction with squaric acid or its ethylester. In the case of CN2 and CN4, ethyl squarate has been modified by a Knoevenagel reaction. The bromo-squaraines have been reacted through a Buchwald-Hartwig reaction to introduce the diphenyl-amino moiety. Carboxylic groups were protected as tert-butyl ester and deprotected by trifluoroacetic acid to yield the final products bearing two or four carboxyl-anchoring groups – Scheme 1. See the supporting information (SI) for a more detailed description of the synthetic pathway.

Theoretical, photophysical, and electrochemical characterizations

The stereoisomerism is expected to govern the performance of SQ sensitized p-type DSSCs, since it induces peculiar HOMO and LUMO electronic charge distribution and it is responsible of the sensitizer adsorption mode and orientation on the semiconductor. Thus, our first step was to perform density functional theory (DFT) calculations, see SI for computational details, to determine the relative stabilities of the *cis/trans* conformers of **O4** and **CN4**. Calculations showed that *trans*-**O4** is only 0.65 kcal/mol more stable than *cis*-**O4**, while the *cis*-**CN4** is 5.40 kcal/mol more stable that the *trans*-isomer. Based on the computed energy stabilities,
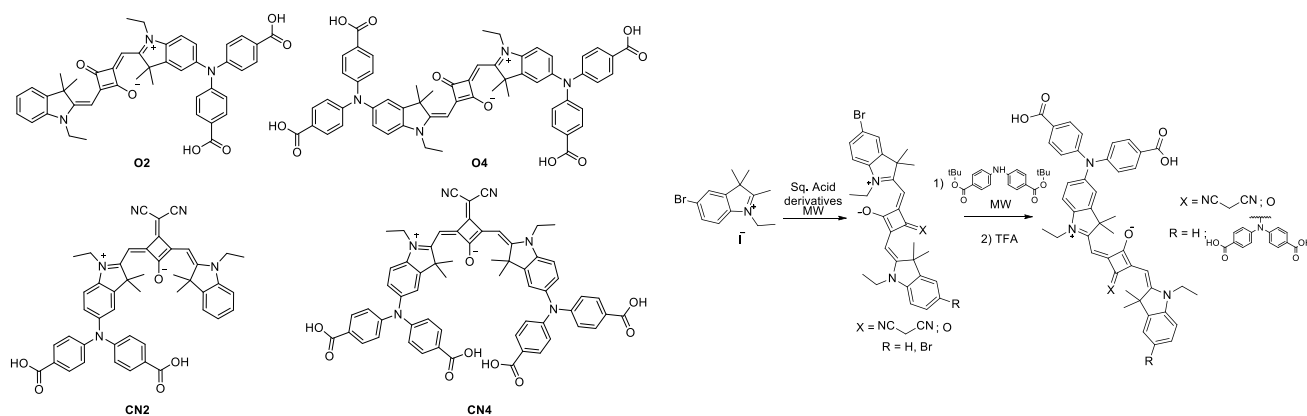
Scheme 1 Synthetic pathway of the novel series of SQs.

we can conclude that the CN-functionalized analogues are reasonably locked in the *cis*-configuration due to steric hindrance, while **O4** is likely to be a mixture of the *trans*- and *cis*-isomers. The optimized molecular structures together with the relative energies of all the possible conformers are shown in **Figure S1**. In **Figure 2** the HOMOs and LUMOs of the optimized SQs are shown. Interestingly, the HOMO is mainly localized on the squaraine core extending up to the fused phenyl rings and at first glance, all the HOMOs appear quite similar. A closer look reveals, however, that the presence of the CN groups concentrates the electronic distribution on the center of the molecule.
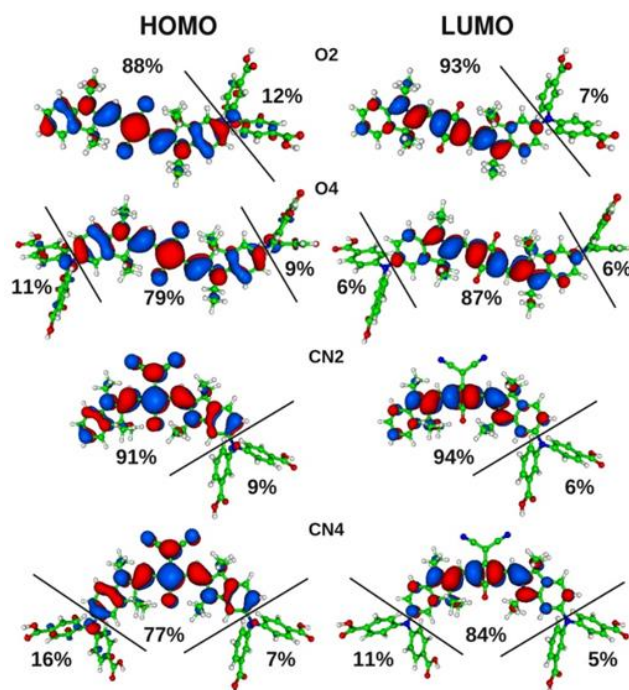

Figure 2. HOMO (left) and LUMO (right) isodensity plots of **O2**, **O4**, **CN2**, and **CN4** including the percentage of electron density associated with the different molecular fragments.

The strong electron-withdrawing CN groups in **CN2** and **CN4** enhance the electron accepting character of the squaraine core and, as such, tune the electronic distribution of the sensitizer.[24] The LUMOs are essentially localized on the squaraine core. Here, the biphenylamines and the dicyanovinyls have, at best, a marginal impact. In addition, we computed the electron density difference between the singlet excited state S_1 and the ground state S_0 in ethanol – see **Figure 3**. In the excited state, the positive charge distribution (red isosurface in **Figure 3**) is in part localized close to the NiO-anchoring groups. In other words, such a charge distribution is likely to favor hole injection from the SQ excited state to the NiO valence band. Please note that this finding is in agreement with the electrochemical characterization, *vide infra*. To confirm the electron-accepting character of the novel class of SQs, cyclic voltammetry assays were performed – **Figure S2**. Two quasi-reversible oxidations centered at around +0.59 and

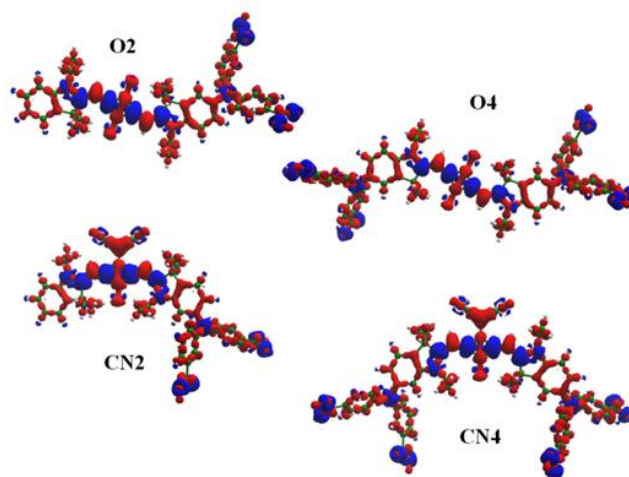**Figure 3.** Isodensity plots of the electron density difference in ethanol solution between the S_1 and the S_0 ground state of all the investigated SQs. The red/blue colors indicates a decrease/increase of the electron density upon excitation.

+0.70 V as well as one quasi-reversible reduction in the range from -0.71 to -0.98 V were noted for all SQs (**Table 1**). Owing to the fact that **O2**, **O4**, **CN2**, and **CN4** give rise to similar reduction features, only minor, if any, differences in the charge injection and electrolyte regeneration driving forces are expected. To solidify this notion, **Figure S3** displays an energy diagram gathering the redox features of the SQs along with the Fermi level energy of NiO (+0.5 V)[25] and the redox potential of the I^-/I_3^- redox couple (+0.34 V).[26] Our analyses suggest that both the electron injection from NiO to the excited state of all SQs and the SQ regeneration by the electrolyte are thermodynamically feasible. The only exception is **CN2**, which shows a moderate driving force of only -0.09 V for the charge injection process - **Figure S3**. As a matter of fact this is one of the reasons for the low short-circuit current density (J_{sc}) and the poor IPCE – *vide infra.* **Figure 4** and **Table 1** summarize the absorption characteristics of the investigated SQs in solution and on NiO electrodes. **O2** and **O4** show two distinct absorptions at 325 nm (ε = 8,000 $M^{-1}cm^{-1}$) and 650 nm (ε = 57,100 $M^{-1}cm^{-1}$) and at 325 nm (ε = 22,600 M^{-1} cm^{-1}) and 674 nm (ε = 84,600 M^{-1} cm^{-1}), respectively, ascribable to the S_2 (high-energy region) and the S_1 (low- energy region) transitions.[27] The increased extinction coefficient (ε) and the red-shifted absorption spectrum stem from the introduction of a second biphenylamine-moiety and the corresponding change in symmetry, that is, from asymmetric to symmetric. In addition to a general bathochromic shift, a new shoulder emerges at 415 and 400 nm for **CN2** and **CN4,** respectively. Time-dependent DFT calculations (TD-DFT) are consistent with the experimental findings – **Table 1**. In particular, the low-energy region of the absorption spectra is attributed to a HOMO→LUMO transition. For the **O4**, **CN2**, and **CN4**, the feature in the high-energy region relates to combinations of transitions involving HOMO and HOMO-1 to LUMO, LUMO+2, and LUMO+5 – **Table 1**, while for **O2** it is due to a single transition with a distinct HOMO-1→LUMO+1 character. For the CN-family, we compute –
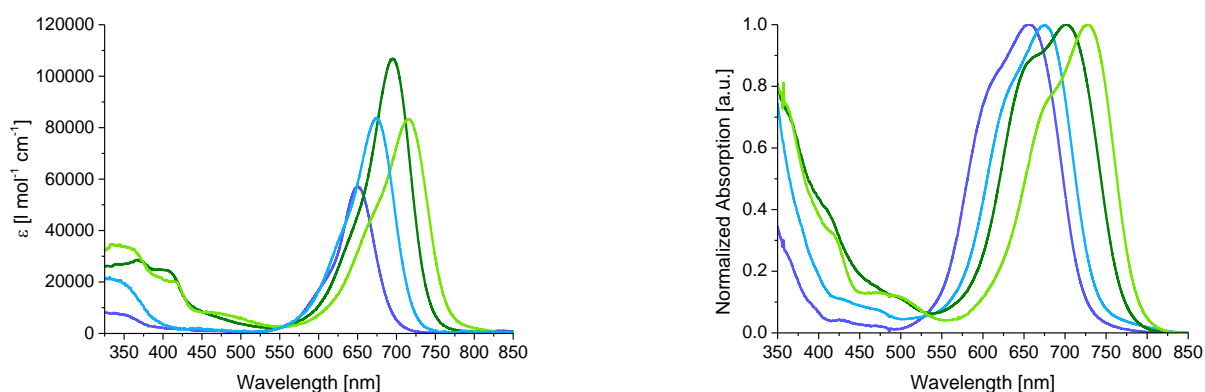

Figure 4. Absorption spectra of **O2** (violet), **O4** (blue), **CN2** (green), and **CN4** (light-green) in ethanol (top) and adsorbed onto mesoporous NiO electrodes (bottom).

in line with the experimental observation – an intermediate band at around 400 nm attributed to a single transition from either HOMO-2 or HOMO-3 to LUMO. Finally, since the presence of the CN-moiety forces the SQ bridge into a *cis*-conformation – *vide supra* – a lower ε in the case of **CN4** was noted compared to that of **CN2**. Corroborating this finding, the extinction coefficient of **O4** increases compared to **O2** as theoretically both the *cis*- and *trans*-conformers are present in solution.

Moreover, the absorption on NiO electrodes was studied – **Figure 4**. Overall, a broadening of the absorption for all SQs and a further red-shift of the maxima due to their binding to NiO electrode surfaces were noted.[28] We ascribe the high-energy shoulder to thermal and solvent fluctuations as noted in previous theoretical studies on SQ / TiO$_2$ electrodes.[29] More interestingly, the red-shift increases in the order **O4** (1 nm) < **O2** (5 nm) < **CN2** (6 nm) < **CN4** (13 nm). In previous studies, it was documented that the extend of red-shift scales with the strength of interactions with the electrode.[28,30] Thus, this finding points to a possibly better injection efficiency of **O2** compared to **O4**, as well as for **CN4** compared to **CN2.**

Table 1. Absorption maxima in solution (λ_{abs}) with their molar extinction coefficient (ε), computed absorption maxima (computed λ_{abs}) with their oscillator strengths, nature of the transition, absorption maxima on NiO electrodes (λ_{NiO}), calculated zero-zero transition energy (E_{0-0}), and redox potentials of the investigated SQs.

Dye	λ_abs [nm] (ε x 10^4 M^-1 cm^-1)^a	Computed λ_abs [nm] (osc. str.)	Composition^b	λ_NiO [nm]	E_{0-0}^c [eV]	Ox_1^d [V]	Ox_2^d [V]	Red^d [V]
O2	325 (0.80)	338 (0.31)	86% H-1→L+2	655	1.77	+0.69	+0.95	-0.87
	650 (5.71)	586 (1.92)	99% H→L					
O4	325 (2.26)	342 (0.25)	73% H-1→L+3	675	1.71	+0.60	+0.85	-0.98
			14% H-2→L+3					
		366 (0.46)	64% H-1→L+1					
			30% H-2→L+1					
	674 (8.46)	611 (2.15)	99% H→L					
CN2	337 (2.40)	315 (0.21)	67% H→L+5	701	1.67	+0.59	+0.80	-0.85
		346 (0.37)	88% H-1→L+2					
	415 (1.46)	368 (0.27)	82% H→L+3					
		421 (0.55)	92% H-2→L					
	695 (10.72)	613 (1.25)	99% H→L					
CN4	366 (2.86)	360 (0.28)	43% H-2→L+1	727	1.61	+0.70	+0.89	-0.71
			28% H→L+5					
			21% H-1→L+1					
		375 (0.36)	87% H→L+4					
	400 (2.48)	402 (0.61)	93% H-3→L					
	714 (4.87)	639 (1.42)	99% H→L					

[a] EtOH solutions. [b] This is provided in terms of molecular orbitals with contribution above the 10%. [c] Calculated from the abscissa of the absorption edge with $E_{0-0} = 1238.9/\lambda$. [d] Referenced vs. NHE with $E(F_c/F_c^+)$ as 0.64V *vs.* NHE.[31]

p-type DSSC characterization

Next, we assembled p-type DSSCs with NiO-based photocathodes sensitized with the four different SQs. NiO electrodes have been prepared according to literature procedures.[32] After sintering, the electrodes were immersed for 16 h into 0.1mM ethanolic solutions of the SQs. Devices were completed with a platinum counter electrode and filled with an electrolyte based on 1 M LiI and 0.2 M I_2 in acetonitrile.

The J-V curves and IPCE spectra are shown in **Figure 5**, while the device figures-of-merit are gathered in **Table 2**. Devices have been measured under dark and 1 sun AM 1.5 conditions. As shown in **Figure 5**, the open-circuit voltages (V_{oc}s) and J_{sc}s decrease from 100.0 to 97.5, to 87.7, and to 85.3 mV and from 1.54 to 1.21, to 1.15, and to 0.94 mA/cm² for devices featuring **O2**, **O4**, **CN4**, and **CN2**, respectively. With almost equal fill factors (FFs) of around 0.35-0.37, the efficiencies differed greatly, namely 0.054% (**O2**), 0.043% (**O4**), 0.029% (**CN2**), and 0.037% (**CN4**). In terms of IPCE, a perfect agreement with the absorption features as shown in **Figure 4** was noted. In the high-energy region, the maximum is mostly dominated by the absorption of the iodine/iodide redox couple, while in the low-energy region, the feature matches with the S_1 transition of the corresponding SQs with values of 8.6% 3.7%, 3.2%, and 3.0% for **O2**, **CN4**, **CN2**, and **O4**, respectively. To verify the comparability of our results, we looked into the dye loading of all devices. As a matter of fact,
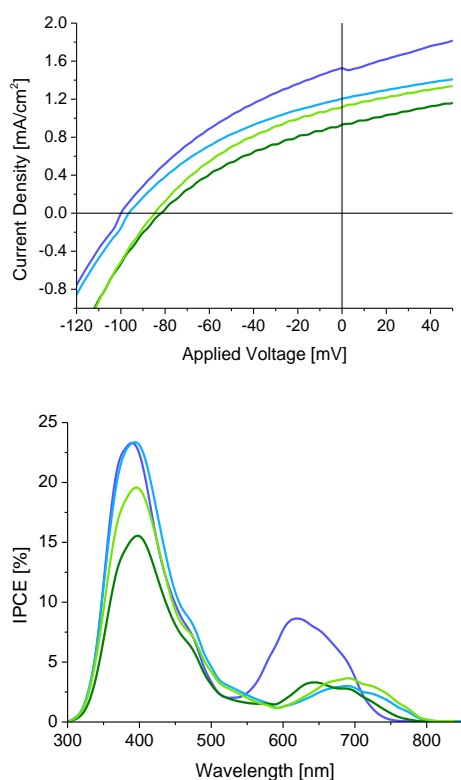
Figure 5. Current density *versus* applied voltage (top) and incident photon-to-current conversion efficiency (bottom) of devices with **O2** (violet), **O4** (blue), **CN2** (green), and **CN4** (light-green).

Table 2. Figures-of-merit for **O2**, **O4**, **CN2**, and **CN4** p-DSSCs.

Dye	V_{oc} [mV]	J_{sc} [mA/cm^2]	FF	η [%]	IPCE [%][a]	Dye loading [mol/cm^2][b]
O2	100.0	1.54	0.35	0.054	8.6	$1.43 \pm 0.19 \times 10^{-8}$
O4	97.5	1.21	0.36	0.043	3.0	$2.02 \pm 0.19 \times 10^{-8}$
CN2	85.3	0.94	0.36	0.029	3.2	$0.47 \pm 0.04 \times 10^{-8}$
CN4	87.7	1.15	0.37	0.037	3.7	$0.66 \pm 0.12 \times 10^{-8}$

[a] Values taken at the corresponding IPCE maxima in the low-energy region of the spectra. [b] Determined from an average of 5 sensitized electrodes.

the concentrations decrease in the order from 2.02×10^{-8} (**O4**), to 1.43×10^{-8} (**O2**), to 0.66×10^{-8} (**CN4**), and to 0.47×10^{-8} M (**CN2**). In this context, it seems more decisive to compare SQs with and without the CN moiety rather than the number of anchoring groups. From the aforementioned figures-of-merit, it is clear that devices sensitized with **O2** outperform any other device, while the increase of anchoring groups (**O4**) correlates with a decrease of the device parameters. In stark contrast, the opposite has been observed for the **CN** family. Here, **CN4** exhibits a better efficiency, as well as higher V_{oc}s and J_{sc}s compared to **CN2** based devices. Helpful is in this regard the structural conformation and the different dye loading of the SQs on the NiO electrodes.

According to the theoretical calculations, **O4** is slightly more stable in its *trans*-conformation. With a seemingly equal dye loading – **Table 2** – it is reasonable to assume that both **O2** and **O4** similarly attach with two linkers upright in a tight manner onto the electrode surface. In stark contrast, **CN4** is most stable in its *cis*-conformation – **Figure 2**– and, thus, both dyes absorb onto NiO in a more bulky manner with either two in the case of **CN2** or with four linkers in the case of **CN4**. These considerations assist in rationalizing a three times lower dye loading relative to **O2** and **O4**.

However, both the trend in J_{sc} and η noted in the O-family and the differences in the η between O- and CN-devices cannot be fully explained by the dye loading. For instance, devices with **O2** and **CN2** dyes showed that the former gives rise to a superior performance in terms of V_{oc}, J_{sc}, and efficiency. This is likely to relate to a higher amount of dye uptake, but an alternative rationale for the lower efficiency of **CN2** devices might include the unfavorable charge shift from the CN-moiety to the SQ core and, in turn, closer to the anchoring group.

As such, charge recombination between the reduced form of **CN2** and the semiconductor surface is facilitated – **Figure 2**. The **O2** *versus* **CN2** trend is in sharp contrast to the **O4** *versus* **CN4** trend. Despite a superior dye uptake in the case of **O4**, both devices show nearly the same J_{sc}. Here, we hypothesize that a more efficient charge collection by virtue of a binding motif that consists of four anchoring groups rather than two is the cause for the reversed trend. Finally, the **CN2** *versus* **CN4** comparison leads to the same trend.

Again, despite comparable dye uptake, four anchoring groups, which are locked into a *cis*-conformation, result in superior charge collection properties.

To corroborate our hypotheses, we turned to electrochemical impedance spectroscopy (EIS) assays. These enabled probing the charge injection and recombination processes under device operation conditions – **Figure 6**.[33–35] In a Nyquist plot for the p-type DSSC, two semicircles correlate with the resistance across the dye/electrode/electrolyte interface in the low-frequency region and with the platinum/electrolyte interface in the high-frequency region.[35,36] The electrical circuit model that has been used for the fitting of the obtained Nyquist plots and the calculation of the resistances is shown in **Figure S4**. Under 1 sun AM 1.5 and J_{sc} conditions, the charge-transfer resistance (R_{CT}) clearly relates to the charge injection, since the device runs under maximum photocurrent generation and, thus, recombination is at its minimum.[34,35] The R_{CT}s under J_{sc} conditions are 669.2, 648.4, 879.9, and 662.7 Ω for **O2**, **O4**, **CN2**, and **CN4** based-DSSCs, respectively.

Taking the aforementioned into concert, three major conclusions are derived. Firstly, **O2** and **O4** show comparable R_{CT}s, pointing to a similar charge injection. This is only feasible if an analogous attachment onto NiO surfaces is realized – *vide infra*. Therefore, **O4** quite likely attaches *via* only two linkers onto NiO as the **O2** dye, since both *cis*- and *trans*-conformations are energetically similar. Secondly, the presence of a CN-moiety fails to improve
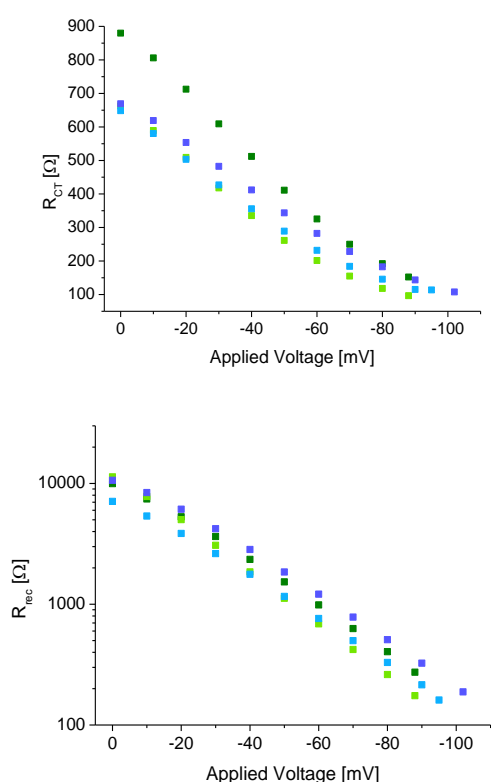

Figure 1. Charge transfer resistance R_{CT} (top) and recombination resistance R_{rec} (bottom) as a function of the applied voltage for **O2** (violet), **O4** (blue), **CN2** (green), and **CN4** (light-green).

the charge injection as R_{CT} is higher for **CN2** than for **O2**. On one hand, the dye uptake is inferior and, in therefore, more charges have been injected for **O2**. On the other hand, a charge shift in **CN2** might bring the electron closer to the anchoring group. Thirdly, a nearly 25% higher R_{CT} for **CN2** than for **CN4** points to the superior charge injection process for the later due to the presence of four anchoring groups, which engage in the adsorption owing to the fact the *cis*-conformation is locked.

Next, EIS assays were performed under dark conditions to gain insights into the recombination resistance (R_{rec}), which mainly correlates with the recombination process between the NiO electrode and the electrolyte. The highest R_{rec} under J_{sc} conditions, namely the least recombination, is found for devices with **CN4** (11,336 Ω) followed by **O2** (10,617 Ω), **CN2** (9,959.8 Ω), and **O4** (7,095.7 Ω). Since **CN4** might attach with four anchoring groups, the best surface coverage of the NiO electrodes leads to the fewest recombination sites for the electrolyte. SQs with only two carboxylic anchors, that is, **O2** and **CN2**, show a comparable rate of recombination with the electrolyte despite differences in the dye uptake. The bulkiness of **CN2** as a means to shield the NiO surface equally good as the more tightly packed **O2,** due to a higher dye loading**,** seems reasonable. In stark contrast, **O4** shows the highest recombination rate as reflected by a R_{rec} 40% lower compared to **CN4**. Here, an incomplete attachment involving only two rather than four anchoring groups might dominate. This would involve one biphenylamine-moiety, which, for example, points toward the bulk of the electrolyte.

From the EIS measurements under dark and 1 sun AM 1.5 conditions, the effective diffusion length (L_{eff}) and the charge collection efficiency (η_{cc}) have been derived – **Figure S5**.[33,35,37] L_{eff} and η_{cc} give insights into the ratio of charge injection and recombination of the investigated devices. The earlier is a measure of how far the injected holes travel inside the mesoporous NiO electrode prior to the recombination process, while the latter relates to the amount of injected holes that are collected at the back contact of the device. All devices show increasing L_{eff}s and η_{cc}s upon decreasing the applied voltage. As a matter of fact, this is characteristic for p-type DSSCs.[33,35] Under V_{oc} conditions, **CN4** shows the longest L_{eff} with 1.21 µm, which decreases to 0.99, to 0.93, and to 0.86 µm for **O2**, **O4**, and **CN2**, respectively. Under the same conditions, η_{cc} increases in the order of 29.3 (**O4**), 42.6 (**O2**), 44.4 (**CN2**), and 44.9 % (**CN4**). Considering these parameters, the use of four anchoring groups seems to be only beneficial if the system is locked into a *cis*-conformation (**CN4** *versus* **O4**).

After gaining an insight into the charge injection and recombination properties of our devices, we have to point out the limitations of our EIS measurements. While it is an excellent tool to study the aforementioned processes, it is unsuitable for probing the recombination between the excited dye anion and the NiO semiconductor. The latter has been identified as one of the major loss mechanism in NiO-based p-type DSSCs which severely limits the achievable FFs.[38,39] At this point we were unable to probe this process for our devices. Owing to the similar dye architecture and electron distributions shown for both HOMO and LUMO levels, we expect a comparable dye-NiO recombination for all of the investigated SQs. Nevertheless, further electrochemical and transient absorption spectroscopy studies are needed to clarify this notion.

Next, we turned to test the suitability of SQ / NiO photocathodes in t-DSSCs. We assembled t-DSSCs consisting of N719 / TiO$_2$ photoanodes as the 300 to 600 nm absorbing sensitizer, and **O2** / NiO photocathodes as the 600 to 750 nm absorbing sensitizer. Here, an acetonitrile-based electrolyte (i.e., 1 M LiI, 0.1 M I$_2$, and 0.5 M 4-*tert*-butylpyridine to suppress recombination on the TiO$_2$ electrode)[26] was used. J-V curves and IPCE spectra of the N719 / TiO$_2$ n-DSSC and **O2** / NiO p-DSSC, as well as the TiO$_2$ / N719 / **O2** / NiO t-DSSC are depicted in **Figure 7** and the device-figures-of-merit are summarized in **Table 3**.

Table 3. Figures-of-merit for the N719/TiO$_2$ and O2/NiO reference devices and the respective t-DSSC illuminated from the TiO$_2$ and NiO side.

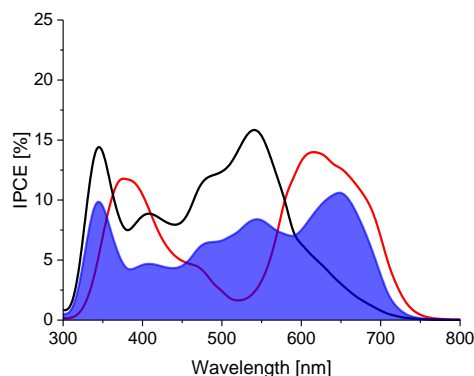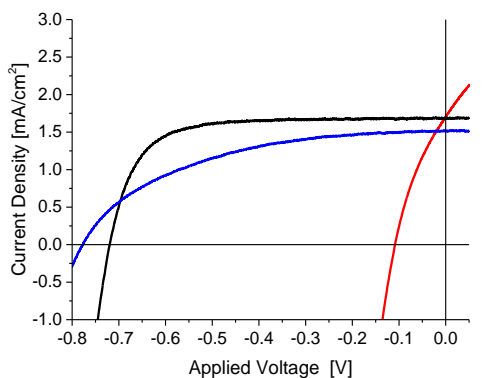| Device	V_{oc} [mV]	J_{sc} [mA/cm^2]	FF	η [%]
N719/TiO$_2$	719.0	1.68	0.73	0.88
O2/NiO	109.7	1.70	0.33	0.062
t-DSSC TiO$_2$ side	777.6	1.51	0.50	0.58

Figure 7. Current density *versus* applied voltage (top) and incident photon-to-current conversion efficiency (bottom) of the TiO$_2$ (black) and NiO (red) reference devices and the respective t-DSSC illuminated from the TiO$_2$ side (blue).

Special attention has been directed to match the photocurrents of both photoelectrodes. This was achieved by reducing the electrode thickness of the TiO$_2$-based photoanode – please see the SI for a more detailed description of the device preparation. N719 / TiO$_2$ n-DSSC and **O2** / NiO p-DSSC show V_{oc}s of 719.0 and 109.7 mV, J_{sc}s of 1.68 and 1.70 mA/cm^2, FFs of 0.73 and 0.33, and efficiencies of 0.88 and 0.062 %, respectively. In contrast, TiO$_2$ / N719 / **O2** / NiO t-DSSC shows a V_{oc} of 777.6 mV, a J_{sc} of 1.51 mA/cm^2, a FF of 0.50, and an efficiency of 0.58 % upon illumination from the TiO$_2$ side. Most importantly, as reported in the literature, the V_{oc} of the t-DSSC is higher than those of the n-and p-DSSCs.[2–4] We note that the efficiencies of the t-DSSCs are slightly lower than those of the TiO$_2$-based n-DSSCs. Quite likely, this is related to the moderate FF due to an inherent problem of NiO-based p-type DSSCs as discussed in recent literature.[33,38] Of far more greater importance is, however, the IPCE spectrum of the t-DSSCs: both N719 and **O2** equally contribute to the photogenerated current. As such, a panchromatic light-harvesting, which ranges from 300 to *ca.* 750 nm (**Figure 7**), evolves and, which perfectly fits to the overlap of the N719 and **O2** absorption features.

Conclusions

A novel family of SQs for p-type DSSCs, which differ in the number of carboxylic anchoring groups and their conformation due to the introduction of a CN central group, has been synthesized and characterized by means of steady-state photophysical, electrochemical, and computational techniques. DSSCs based on NiO photocathodes and SQs have been assembled and tested. The different conformations of the SQs governed the adsorption onto the electrode surface, which was directly reflected in the dye loading and device efficiency. As a complement, EIS assays were performed to probe the impact of the molecular structures on the electron injection and recombination processes in the device. Here, our findings revealed superior charge injection and recombination properties for SQs featuring four anchoring groups (**CN4**) only when a frozen *cis*-conformation is guaranteed. As a complement, we assembled for the first time a t-DSSC based on a SQ / NiO and N719 / TiO$_2$, which harvests light throughout most of the visible spectrum. Future investigations will involve the synthesis and characterization of symmetric SQ sensitizers to further enhance the charge injection properties under device operation conditions, as well as, the further electrolyte optimization of SQ-based t-DSSCs.

Experimental Section

1. Computational Methodology

DFT[40] and TDDFT[41,42] calculations have been carried out with the Gaussian 09 package.[43] Geometry optimizations, with no symmetry constraints, have been performed using B3LYP hybrid functional[44–46] and 6-311G* basis set[47,48] in vacuo. Frequency calculations have been performed at the same level of calculation on the optimized geometry to verify the nature of the computed geometries. The first 100 singlet-singlet excitations have been computed using TD-DFT in dichloromethane solution. Solvent effects have been taken into account, using the non-equilibrium Conductor-like Polarization Model, CPCM solvation model.[49] Using the transition energies and the oscillator strengths, the spectra have been simulated by using a Gaussian convolution with a σ of 0.1 eV.

2. Photophysical and electrochemical characterization

Steady-state absorption spectra were recorded with a Perkin-Elmer Lambda 35 spectrophotometer. The extinction coefficient was determined three times for each of the corresponding dyes to ensure the reproducibility of our results. Desorption of the SQ-dyes was performed by immersing the sensitized NiO electrodes for 1h in acetic anhydride. Cyclic voltammetry assays of the corresponding dyes (c = 1 x 10^{-4} M) were performed in DMSO, on a Metrohm µAutolabIII potentiostat with a platinum wire as counter electrode, an Ag wire as pseudo-reference electrode and a glassy carbon working electrode.

3. Preparation and characterization of p-type DSSCs and t-DSSCs

A NiO precursor solution was prepared by mixing NiCl$_2$ (1g), a triblock co-polymer F108 (1g), Milli-Q water (3g) and ethanol (6g). The obtained solution was stirred until a transparent green precursor was obtained. After 3 days of resting at 30°C the solution was centrifuged to remove any remaining crystallites before being used for doctor blading. For the preparation of the TiO$_2$ electrodes for the application in t-DSSCs the standard paste from Solaronix (Ti-Nanoxide T/SP), which was diluted with ethanol to obtain thinner films, was used.

As substrates for the NiO and TiO$_2$ electrodes fluoride doped tin oxide glass slides (FTO, 8 Ω/square, Pilkington, XOP Glass) were used which were washed by ultrasonication in solutions of acetone, tenside solution, water, and isopropanol for 15 minutes each. Afterwards, the FTO slides were cleaned in an ozone lamp cleaner (Jelight company, Inc.) for 18 minutes. The NiO precursor and the diluted TiO$_2$ paste were applied by doctor blading onto the FTO substrates with the help of a Scotch tape mask (total area of the electrode was 0.2 cm^2). Afterwards the electrodes were calcinated at 450°C or 550°C for 30 minutes for the NiO and TiO$_2$ based electrodes, respectively. For the NiO electrodes, this process was repeated a second time to obtain double layered NiO electrodes. The still hot electrodes (roughly 80°C) were immersed for 16h into the corresponding dye solutions, namely the SQ sensitizers for NiO (c = 1 x 10^{-4} M in ethanol) and N719 (Sigma-Aldrich) for TiO$_2$ (c = 3 x 10^{-4} M in tert-butanol:acetonitrile as 1:1 v/v). The thickness of the electrodes was determined to be 1.2 - 1.4µm (NiO) or 0.75 µm (TiO$_2$) in average with a profilometer (Bruker OM DektakXT).

The NiO and TiO$_2$-based devices were completed by pressing a Pt counter electrode (5 mM H$_2$PtCl$_6$ on FTO baked at 400°C) and the NiO electrodes with Syrlin (Solaronix 25μm) at 150°C. The t-DSSC devices were completed by pressing the TiO$_2$ as photoanode and the NiO as photocathode/counter electrode together with Syrlin at 150°C. The electrolyte, either 1M LiI + 0.2M I$_2$ (for NiO devices) or 1M LiI + 0.1M I$_2$ + 0.5M 4-*tert*-butylpyridine (for t-DSSCs and their respective TiO$_2$ and NiO based reference devices) both in acetonitrile, was filled into the cell through two predrilled holes in the counter electrode which were afterwards sealed with Syrlin foil and an additional glass slide. In order to ensure the reproducibility of our results, five devices have been measured for each of the tested SQ-dyes.

J-V assays in the dark and under 1 sun AM 1.5 standard conditions were performed in a voltage range of -0.8V (TiO$_2$ and t-DSSC devices) or -0.2V (NiO devices) to 0.05V with the help of a Metrohm PGSTAT30 potentiostat. In the case of the NiO-based p-type DSSCs, the counter electrode was connected to the NiO photocathode and the working electrode to the platinum counter electrode. For the TiO$_2$-based n-type DSSCs and the t-DSSCs the working electrode was connected to the TiO$_2$ photoanode and the counter electrode to the NiO photocathode (t-DSSC) or platinum based counter electrode (TiO$_2$ n-type DSSC). Electrochemical impedance spectroscopy (EIS) assays have been performed with a small voltage amplitude of 10mV in a frequency range of 100 kHz to 10 mHz. Multiple EIS measurements have been performed for each device starting at V$_{oc}$ conditions and then going down in 10 mV steps till the J$_{sc}$ condition has been reached. With the help of an appropriate model (**Figure S4**), the obtained Nyquist plots have been fitted to extract the impedance parameters.[36] Incident-photon-to-current efficiency (IPCE) measurements have been performed in a spectral range of 300 to 850 nm. Here, the device was illuminated from the side of the NiO/TiO$_2$ electrode, if not stated otherwise, with a xenon arc lamp over a Cornerstone 260 1/4m Monochromator equipped with a Merlin digital radiometric lock-in-system.

Acknowledgements

[1]   B. O'Regan, M. Grätzel, *Nature* **1991**, *353*, 737–740.

[2]   A. Nattestad, A. J. Mozer, M. K. R. Fischer, Y. Cheng, A. Mishra, P. Bäuerle, U. Bach, *Nat. Mater.* **2010**, *9*, 31–35.

[3]   S. Powar, R. Bhargava, T. Daeneke, G. Götz, P. Bäuerle, T. Geiger, S. Kuster, F. A. Nüesch, L. Spiccia, U. Bach, *Electrochim. Acta* **2015**, *182*, 458–463.

[4]   C. J. Wood, G. H. Summers, E. A. Gibson, *Chem. Commun.* **2015**, *51*, 3915–3918.

[5]   E. A. Gibson, A. L. Smeigh, L. Le Pleux, J. Fortage, G. Boschloo, E. Blart, Y. Pellegrin, F. Odobel, A. Hagfeldt, L. Hammarström, *Angew. Chemie, Int. Ed. Engl.* **2009**, *48*, 4402–4405.

[6]   X. L. Zhang, Z. Zhang, D. Chen, P. Bäuerle, U. Bach, Y.-B. Cheng, *Chem. Commun.* **2012**, *48*, 9885–9887.

[7]   I. R. Perera, T. Daeneke, S. Makuta, Z. Yu, Y. Tachibana, A. Mishra, P. Bäuerle, C. A. Ohlin, U. Bach, L. Spiccia, *Angew. Chemie Int. Ed.* **2015**, *54*, 3758–3762.

[8]   E. Sheibani, L. Zhang, P. Liu, B. Xu, E. Mijangos, G. Boschloo, A. Hagfeldt, L. Hammarström, L. Kloo, H. Tian, *RSC Adv.* **2016**, 18165–18177.

[9]   Y. Farré, L. Zhang, Y. Pellegrin, A. Planchat, E. Blart, M. Boujtita, L. Hammarström, D. Jacquemin, F. Odobel, *J. Phys. Chem. C* **2016**, *120*, 7923–7940.

[10]   L. Zhang, L. Favereau, Y. Farre, A. Maufroy, Y. Pellegrin, E. Blart, M.- Hissler, D. Jacquemin, F. Odobel, L. Hammarström, *RSC Adv.* **2016**, *6*, 77184–77194.

[11]   S. Lyu, Y. Farré, L. Ducasse, Y. Pellegrin, T. Toupance, C. Olivier, F. Odobel, *RSC Adv.* **2016**, *6*, 19928–19936.

[12]   A. Sinopoli, C. J. Wood, E. A. Gibson, P. I. P. Elliott, *Dye. Pigment.* **2017**, *140*, 269–277.

[13]   G. H. Summers, J.-F. Lefebvre, F. A. Black, E. Stephen Davies, E. A. Gibson, T. Pullerits, C. J. Wood, K. Zidek, *Phys. Chem. Chem. Phys.* **2016**, *18*, 1059–1070.

[14]   F. Odobel, L. Le Pleux, Y. Pellegrinn, E. Blart, *Acc. Chem. Res.* **2010**, *43*, 1063–1071.

[15]   J. F. Yin, M. Velayudham, D. Bhattacharya, H. C. Lin, K. L. Lu, *Coord. Chem. Rev.* **2012**, *256*, 3008–3035.

[16]   C. Qin, W.-Y. Wong, L. Han, *Chem. Asian J.* **2013**, *8*, 1706–1719.

[17]   C. Chang, Y. Chen, C. Hsu, H. Chou, J. T. Lin, *Org. Lett.* **2012**, *14*, 4726–4729.

[18]   J. Warnan, J. Gardner, L. Le Pleux, J. Petersson, Y. Pellegrin, E. Blart, L. Hammarström, F. Odobel, *J. Phys. Chem. C* **2014**, *118*, 103–113.

[19]   A. Burke, L. Schmidt-Mende, S. Ito, M. Grätzel, *Chem. Commun.* **2007**, 234–236.

[20]   J. Park, C. Barolo, F. Sauvage, N. Barbero, C. Benzi, P. Quagliotto, S. Coluccia, D. Di Censo, M. Grätzel, M. K. Nazeeruddin, et al., *Chem. Commun.* **2012**, *48*, 2782–2784.

[21]   J. Park, N. Barbero, J. Yoon, E. D. Orto, S. Galliano, R. Borrelli, J. Yum, D. Di Censo, M. Gr, K. Nazeeruddin, et al., *Phys. Chem. Chem. Phys.* **2014**, *16*, 24173–24177.

[22]   A. J. Winstead, N. Fleming, K. Hart, D. Toney, *Molecules* **2008**, *13*, 2107–2113.

[23]   N. Barbero, C. Magistris, J. Park, D. Saccone, P. Quagliotto, R. Buscaino, C. Medana, C. Barolo, G. Viscardi, *Org. Lett.* **2015**, *17*, 3306 – 3309.

[24]   F. Odobel, Y. Pellegrin, *J. Phys. Chem. Lett.* **2013**, *4*, 2551–2564.

[25]   J. He, H. Lindström, A. Hagfeldt, L. Sten-Eric, *J. Phys. Chem. B* **1999**, *103*, 8940–8943.

[26]   G. Boschloo, A. Hagfeldt, *Acc. Chem. Res.* **2009**, *42*, 1819–1826.

[27]   U. Mayerhöffer, B. Fimmel, F. Würthner, *Angew. Chemie, Int. Ed.* **2012**, *51*, 164–167.

[28]   P. Qin, M. Linder, T. Brinck, G. Boschloo, A. Hagfeldt, L. Sun, *Adv. Mater.* **2009**, *21*, 2993–2996.

[29]   F. De Angelis, S. Fantacci, R. Gebauer, *J. Phys. Chem. Lett.* **2011**, *2*, 813–817.

[30]   P. Qin, H. Zhu, T. Edvinsson, G. Boschloo, A. Hagfeldt, L. Sun, *J. Am. Chem. Soc.* **2008**, *130*, 8570–8571.

[31]   C. M. Cardona, W. Li, A. E. Kaifer, D. Stockdale, G. C. Bazan, *Adv. Mater.* **2011**, *23*, 2367–2371.

[32]   S. Sumikura, S. Mori, S. Shimizu, H. Usami, E. Suzuki, *J. Photochem. Photobiol. A Chem.* **2008**, *199*, 1–7.

[33]   Z. Huang, G. Natu, Z. Ji, M. He, M. Yu, Y. Wu, *J. Phys. Chem. C* **2012**, *116*, 26239–26246.

[34]   H. Choi, S. O. Kang, J. Ko, G. Gao, H. S. Kang, M.-S. Kang, M. K. Nazeeruddin, M. Grätzel, *Angew. Chemie, Int. Ed.* **2009**, *48*, 5938–5941.

[35]   O. Langmar, C. R. Ganivet, A. Lennert, R. D. Costa, G. de la Torre, T. Torres, D. M. Guldi, *Angew. Chemie, Int. Ed.* **2015**, *54*, 7688–7692.

[36]   Z. Huang, G. Natu, Z. Ji, P. Hasin, Y. Wu, *J. Phys. Chem. C* **2011**, *115*, 25109–25114.

[37]   M. Adachi, M. Sakamoto, J. Jiu, *J. Phys. Chem. B* **2006**, *110*, 13872–13880.

[38]   T. Daeneke, Z. Yu, G. P. Lee, D. Fu, N. W. Duffy, S. Makuta, Y. Tachibana, L. Spiccia, A. Mishra, P. Bäuerle, et al., *Adv. Energy Mater.* **2015**, *5*, 1–11.

[39]   L. D'Amario, L. J. Antila, B. Pettersson Rimgard, G. Boschloo, L. Hammarström, *J. Phys. Chem. Lett.* **2015**, *6*, 779–783.

[40]   P. Hohenberg and W. Kohn, *Phys. Rev.* **1964**, *136*, B864.

[41]   G. E. S. and M. J. F. R. E. Stratmann, *J. Chem. Phys.* **1998**, *109*, 8218.

[42]   K. C. C. and D. R. S. M. E. Casida, C. Jamorski, *J. Chem. Phys.* **1998**, *108*, 4439.

[43]   Gaussian 09, Revision A.1, M. J. Frisch, G. W. Trucks, H. B. Schlegel, G. E. Scuseria, M. A. Robb, J. R. Cheeseman, G. Scalmani, V. Barone, B. Mennucci, G. A. Petersson, H. Nakatsuji, M. Caricato, X. Li, H. P. Hratchian, A. F. Izmaylov, J. Bloino, G. Zheng, J. L. Sonnenberg, M. Hada, M. Ehara, K. Toyota, R. Fukuda, J. Hasegawa, M. Ishida, T. Nakajima, Y. Honda, O. Kitao, H. Nakai, T. Vreven, J. A. Montgomery, Jr., J. E. Peralta, F. Ogliaro, M. Bearpark, J. J. Heyd, E. Brothers, K. N. Kudin, V. N. Staroverov, R. Kobayashi, J. Normand, K. Raghavachari, A. Rendell, J. C. Burant, S. S. Iyengar, J. Tomasi, M. Cossi, N. Rega, J. M. Millam, M. Klene, J. E. Knox, J. B. Cross, V. Bakken, C. Adamo, J. Jaramillo, R. Gomperts, R. E. Stratmann, O. Yazyev, A. J. Austin, R. Cammi, C. Pomelli, J. W. Ochterski, R. L. Martin, K. Morokuma, V. G. Zakrzewski, G. A. Voth, P. Salvador, J. J. Dannenberg, S. Dapprich, A. D. Daniels, Ö. Farkas, J. B. Foresman, J. V. Ortiz, J. Cioslowski, and D. J. Fox, Gaussian, Inc., Wallingford CT, **2009**.

[44]   A. D. Becke, *J. Chem. Phys.* **1993**, *98*, 5648.

[45]   C. Lee, W. Yang and R. G. Parr, *Phys. Rev. B Condens. Matter* **1988**, *37*, 785.

[46]   H. S. and H. P. B. Miehlich, A. Savin, *Chem. Phys. Lett.* **1989**, *157*, 200.

[47]   A. D. McLean and G. S. Chandler, *J. Chem. Phys.* **1980**, *72*, 5639.

[48]   J. A. P. K. Raghavachari, J. S. Binkley, R. Seeger, *J. Chem. Phys.* **1980**, *72*, 650.

[49]   V. B. M. Cossi, N. Rega, G. Scalmani, *J. Comp. Chem.* **2003**, *24*, 669.